



ORIGINAL ARTICLE

# A fast and efficient preparative method for separation and purification of main bioactive xanthenes from the waste of *Garcinia mangostana* L. by high-speed countercurrent chromatography



Ricardo Felipe Alexandre de Mello <sup>a,b,\*</sup>, Wandson B. de Souza Pinheiro <sup>c</sup>,  
Jaisielle Kelem F. Benjamim <sup>a,b,\*</sup>, Francilia Campos de Siqueira <sup>d</sup>,  
Renan Campos Chisté <sup>d</sup>, Alberdan Silva Santos <sup>a,b,\*</sup>

<sup>a</sup> Laboratory of Systematic Research in Biotechnology and Molecular Biodiversity, 01 Augusto Corrêa Street, Guamá, ZIP Code 66075-110 Belém, Pará, Brazil

<sup>b</sup> Institute of Exact and Natural Sciences, Federal University of Pará, 01 Augusto Corrêa Street, Guamá, ZIP Code 66075-110 Belém, Pará, Brazil

<sup>c</sup> Faculty of Chemical Engineering, Institute of Technology, Federal University of Pará, 01 Augusto Corrêa Street, Guamá, ZIP Code 66075-110 Belém, Pará, Brazil

<sup>d</sup> Faculty of Food Engineering, Institute of Technology, Federal University of Pará, 01 Augusto Corrêa Street, Guamá, ZIP Code 66075-110 Belém, Pará, Brazil

Received 18 April 2021; accepted 1 June 2021

Available online 6 June 2021

## KEYWORDS

Bioactivity;  
Mangosteen;  
Agricultural by-products;  
Antioxidant capacity;  
Counter current chromatography separation

**Abstract** In this work, we present a preparative elution method by high-speed countercurrent chromatography (Prep-HSCCC) for the separation and isolation of the main bioactive xanthenes present in the alcoholic extract of *Garcinia mangostana* L. agro-industrial waste. The method proved to be quite efficient, operating with a two-phase solvent system consisting of Methanol/water/Ethanol/Hexane/methyl *tert*-butyl ether (6:3:1:6:4v/v), tail-head elution mode, with mobile phase flow of 5 mL/min and rotation speed of 800 rpm. The method demonstrated repeatability (RSD = 3.8–6.5%) and allowed the isolation of  $\alpha$ -mangostin and  $\gamma$ -mangostin xanthenes, both with purities above 93%, in a single step, performed in a time of 35 min. Isolated substances were

\* Corresponding authors at: Laboratory of Systematic Research in Biotechnology and Molecular Biodiversity, Institute of Exact and Natural Sciences, Federal University of Pará, 01 Augusto Corrêa Street, Guamá, ZIP Code 66075-110 Belém, Pará, Brazil.

E-mail addresses: [ricardofamello@gmail.com](mailto:ricardofamello@gmail.com) (R.F.A. de Mello), [jaisequimica@gmail.com](mailto:jaisequimica@gmail.com) (J.K.F. Benjamim), [alberdan.ufpa@gmail.com](mailto:alberdan.ufpa@gmail.com) (A.S. Santos).

Peer review under responsibility of King Saud University.



identified by HPLC-PDA-MS and  $^1\text{H}$  and  $^{13}\text{C}$  NMR spectroscopy. Both xanthenes were efficient scavengers of DPPH $\cdot$  and ABTS $\cdot^+$  radicals in a concentration-dependent manner with EC $_{50}$  at 8.43 and 3.31  $\mu\text{g/mL}$ , respectively, for  $\gamma$ -mangostin, and 71.10 and 29.33  $\mu\text{g/mL}$ , respectively, for  $\alpha$ -mangostin.

© 2021 The Authors. Published by Elsevier B.V. on behalf of King Saud University. This is an open access article under the CC BY-NC-ND license (<http://creativecommons.org/licenses/by-nc-nd/4.0/>).

## 1. Introduction

Since the early 1980s, organic waste from agribusiness has been a major source of environmental contamination, but it has also been a promising source of products with high value-added. The processing of fruits and vegetables by agro-industrial activity produces, throughout the world, throughout its entire production chain, millions of tons of waste consisting of bagasse, peels, seeds, pulps and even the whole fruit that, when discarded and accumulated inappropriately in the environment, may perform as a continuous source of organic pollution, causing serious environmental problems (Cheok et al., 2018; Yusuf, 2017). Because they are rich in water and biodegradable organic compounds, the decomposition of these waste favors the proliferation of microorganisms that alter the local ecosystem, release a fetid odor and greenhouse gases, in addition to attracting a number of other animals and pests such as mice, cockroaches, flies, among others (Cheok et al., 2018).

Food and Agriculture Organization (FAO) estimates that the production of agro-industrial waste and losses, occurring along of the all food supply chain, can reach between 25 and 30% (FAO, 2019). However, these by-products still reserve large amounts of nutrients, vitamins, minerals, fibers and a multitude of bioactive compounds such as phenolic compounds and other substances with high antioxidant potential, among other properties beneficial to health (Fierascu et al., 2019; Filho and Franco, 2015; Leyva-López et al., 2020; Torres-León et al., 2018; Yusuf, 2017).

In view of the environmental problem surrounding this theme, and of all its therapeutic and economic potential, there is an urgent demand for studies to develop strategic methodologies for management, treatment and processing of these organic waste for generation of products and inputs of high value-added in a sustainable manner (Cheok et al., 2018; Filho and Franco, 2015; Sagar et al., 2018; Yusuf, 2017).

*Garcinia mangostana* Linn (GML), commonly known as mangosteen, is native to Southeast Asia and it is a member of Clusiaceae family (EL-Kenawy et al., 2019; Ketsa and Paull, 2011). It is considered the most admired and tasty tropical fruit in the Asian tropics and it is widely known as the “Queen of fruits” for presenting noble characteristics of texture, aroma and flavor; and for its medicinal properties (Aizat et al., 2019a; EL-Kenawy et al., 2019). Its bark, pericarp and seeds have a long history of use in traditional Southeast Asian medicine (EL-Kenawy et al., 2019; Ketsa and Paull, 2011). Preparations at the base of the pericarp are used in the treatment of various diseases and disorders, such as dysentery, diarrhea; tumors, wounds and bacterial skin infections; diabetes, hypertension and arthritis (EL-Kenawy et al., 2019; Marzaimi and Aizat, 2019). Formulations based on bark and young leaves are effective against diseases and infections of the urinary tract, dysentery, and enteritis (Aizat et al., 2019b; EL-Kenawy et al., 2019; Ketsa and Paull, 2011). Several *in vivo* and *in vitro* evaluation studies of extracts obtained from the pericarp confirmed the existence of a wide variety of bioactive and therapeutic properties (Aizat et al., 2019b; EL-Kenawy et al., 2019; Marzaimi and Aizat, 2019).

Known mainly for its peculiarities and sensory qualities, the mangosteen has been gaining great recognition and prominence internationally (Altendorf, 2018). The fruit is exported to many developed countries where it is offered and marketed as a “superfruit” because it is a rich source of nutrients and bioactive substances with high impact potential against the risks of developing premature aging and

associated degenerative diseases, such as Alzheimer’s, some types of cancer and arteriosclerosis (Altendorf, 2018; EL-Kenawy et al., 2019; Ketsa and Paull, 2011; Shibata et al., 2019).

The traditional use of mangosteen is widely diversified. The fruit is consumed mainly fresh, as a dessert (EL-Kenawy et al., 2019; Ketsa and Paull, 2011; Suttirak and Manurakchinakorn, 2014). However, it is common to produce jellies, purees, jams, wines and preserves from the pulp or the whole fruit. Currently, several products derived from the pericarp and pulp of mangosteen are produced and marketed by food and supplement industry as functional products capable of acting in the prevention of diseases such as diabetes and high blood pressure (Aizat et al., 2019a; de Carvalho, 2014; Sacramento et al., 2007).

GML pericarp is filled with phenolic compounds, such as phenolic acids; flavonoids, including anthocyanins; tannins; and the main ones, isoprenylated xanthenes, derived from dibenzo- $\gamma$ -pyrone, better known as mangostins (EL-Kenawy et al., 2019; Ketsa and Paull, 2011; Suttirak and Manurakchinakorn, 2014). About 70 xanthenes have already been isolated and identified from GML (Aizat et al., 2019a; EL-Kenawy et al., 2019; Ovalle-Magallanes et al., 2017) and at least thirteen of them are found in the pericarp (Yang et al., 2017), being  $\alpha$ -,  $\beta$ - and  $\gamma$ -mangostin, 8-deoxygartanine, gartanine and garcinones C and D the most abundant and, therefore, the most studied (EL-Kenawy et al., 2019; Ovalle-Magallanes et al., 2017). Several *in vitro* and *in vivo* evaluation studies have shown that these compounds are capable of acting on multiple biological targets related to different pathologies (Ovalle-Magallanes et al., 2017). Results revealed a wide variety of intrinsic biological effects, such as antioxidant; antimicrobial, healing; anti-inflammatory and neuroprotective (Aizat et al., 2019b; Chen et al., 2018; Ibrahim et al., 2016; Ovalle-Magallanes et al., 2017); action to control and reduce obesity and disorders associated with metabolic syndrome such as hypertension, diabetes and cardiovascular diseases (Shandiz et al., 2017).

Numerous studies also revealed the antitumor activities of xanthenes extracted from the pericarp against several types of cancer (Aizat et al., 2019b). These compounds were active in leukemia and melanoma models, as well as colon, breast, lung, cervical, prostate carcinomas, among others. This effect is caused by several biological mechanisms, such as induction of apoptosis and autophagy. Other effects against the development of cancer have also been identified, such as the prevention of metastasis and angiogenesis (Aizat et al., 2019b; Ovalle-Magallanes et al., 2017; Shibata et al., 2011; Wang et al., 2017).

The  $\alpha$ -mangostin is the predominant xanthone in the pericarp of the mangosteen (Shan and Zhang, 2010; Walker, 2007; Wittenuer et al., 2012), has an extensive range of biological activities and pharmacological properties, being considered as an antioxidant agent, antimicrobial, antiobesity, anti-inflammatory, anti-hyperglycemic, antidiabetic, antineoplastic, antiproliferative and apoptosis inducer (Chen et al., 2018; Shandiz et al., 2017; Shibata et al., 2011). The  $\alpha$ -mangostin exhibited an inhibiting effect on survival rate and morphological changes in cell lines of tongue mucocarcinoma (TMC), and in mouse melanoma cells. The results of the 3-(4,5-Dimethylthiazol-2-yl)-2,5-diphenyltetrazolium bromide (MTT) assays revealed that the number of viable cells decreased significantly with increasing concentration of  $\alpha$ -mangostin (Lee et al., 2016; Zhou et al., 2021). The analysis of flow cytometry stated that  $\alpha$ -mangostine was capable of suppressing the viability of TMC strains

inducing apoptosis and promoting the interruption of the cell cycle in sub-G1 phase (Lee et al., 2016). A recent study suggests that  $\beta$ -mangostin is able to inhibit the growth of glioma cells, the most common and aggressive malignant tumor of the nervous system, and induce oxidative damage *in vitro*, and inhibit tumor growth *in vivo* (Li et al., 2020). The  $\gamma$ -mangostin, second most abundant xanthone in the pericarp, showed hypoglycemic properties expressing a potent inhibitory activity of the enzyme  $\alpha$ -glycosidase (Wang et al., 2017). Other studies report the apoptotic effects of  $\gamma$ -mangostin on liver cell, colon and glioma malignant cell lines (Ovalle-Magallanes et al., 2017; Wang et al., 2017). Analgesic, anti-inflammatory, antioxidant and neuroprotective effects are also reported for  $\gamma$ -mangostin (Cui et al., 2010; Jaisin et al., 2018). Two others bioactive xanthones present in the mangosteen pericarp are garcinone E and gartinin. Garcinone E showed the ability to inhibit ovarian cancer cells by inducing apoptosis and suppressing the invasion and migration properties of cancer cells, suggesting its potential therapeutic use against ovarian cancer (Xu et al., 2017). Garcinone E also revealed potent antiproliferative activity in cervical, hepatoma, gastric, breast and colorectal cancer cells (Aizat et al., 2019b). Meanwhile, gartinin demonstrated the ability to inhibit cervical and glioma cancer cell lines by interrupting their cell cycle (Aizat et al., 2019b).

Evidence of the antioxidant, neuroprotective, anti-inflammatory and anti-apoptotic properties of mangosteen pericarp also corroborates the application potential of the extract or isolated substances (i.e.  $\alpha$ - and  $\gamma$ -mangosteens) as an alternative adjunctive treatment for severe mental illnesses, generally defined as disorders with psychotic or high-severity symptoms (i.e. bipolar disorder and schizophrenia), diseases that have a low response rate to conventional treatments, and treatment options are limited (Ashton et al., 2019).

Mangosteen pericarp is the main waste generated by the pulp consumption and processing, as it constitutes more than 70% of the fruit mass (de Carvalho, 2014; Chisté et al., 2009; EL-Kenawy et al., 2019; Sacramento et al., 2007). It is estimated that a large amount of this waste is produced worldwide, bringing some environmental impacts that can be reduced or even eliminated by the development of beneficiation and utilization processes of this by-product in the production of bioactive compounds with high therapeutic potential for generation of high value-added products with interest and application in pharmaceutical, foods, dermo-cosmetic, agricultural and medical sectors (Aizat et al., 2019a; Cheok et al., 2018; Yusuf, 2017).

The search for bioactive molecules with applications in several sectors of industry for generation of high value-added products has been the focus of several recent works, and the selection of suitable methods for separation, isolation, and purification of these compounds from natural products and agricultural by-products has shown to be a recurring problem faced by scientific community. The most common separation techniques used in the isolation of metabolites from natural products have some limitations and disadvantages, such as complexity and delay in carrying out the procedures, consumption of significant amounts of solvents, high operational cost, low yields and, in some cases, are poorly reproducible.

High-speed countercurrent chromatography (HSCCC) is a countercurrent chromatography modality (CCC) which was radically improved in terms of resolution, separation time and sample loading capacity, and today, it is a high-efficiency preparatory technique widely used in separation, isolation and purification of natural and synthetic products (Ito, 2005). HSCCC is a liquid-liquid partition chromatography which main difference and advantage in relation to conventional chromatographic methods is the lack of a solid support as stationary phase, which prevents sample losses by irreversible adsorption. Other advantages of the technique are: the great versatility of solvent system, high sample loading capacity, low solvent consumption, high resolution, repeatability, and easy scale-up from micro-gram to tonne (Friesen et al., 2015; Ito, 2005; Luo et al., 2016; Shan and Zhang, 2010). In this sense, the use of HSCCC combined with a quick and efficient procedure of dereplication (Hubert et al., 2017) of the extract by high performance liquid chromatography (HPLC) coupled

with spectroscopic techniques of structural elucidation emerges as a powerful alternative for the development of a strategic workflow of fractionation of natural extracts for isolation and purification, on a preparative scale, of a wide range of classes of compounds with functional properties aimed at production of metabolic concentrates and obtaining substances with great potential for technological application in the generation of high value-added assets (Aizat et al., 2019a).

This work aimed at proposing a simple, fast, and efficient countercurrent separation (CCS) method for obtaining, on a preparative scale, the main bioactive xanthones present in GML pericarp, in addition to evaluating the antioxidant capacity of these compounds.

## 2. Material and methods

### 2.1. Reagents and materials

All organic solvents used in the extractions, chromatographic and spectroscopic processes were of analytical quality: acetonitrile (ACN), dichloromethane ( $\text{CH}_2\text{Cl}_2$ ), chloroform ( $\text{CHCl}_3$ ), diethyl ether, methyl *tert*-butyl ether (MTBE), hexane (Hex), ethyl acetate (EtOAc), anhydrous ethanol (EtOH), methanol (MeOH), in addition to deuterated solvents – chloroform ( $\text{CDCl}_3$ ) and methanol ( $\text{CD}_3\text{OD}$ ), all provided by TEDIA® COMPANY (Fairfield, USA). In the analysis by HPLC-PDA-MS, ultrapure water with resistivity of  $18.3 \text{ M}\Omega/\text{cm}^3$  produced in a purification system of water model Scholar UV UP 900 (BIOHUMAN, Curitiba, Brazil) was used. For preparation of aqueous stationary phase that comprised the two-phase solvent system used in the separation by HSCCC, distilled water was used. For analysis by analytical thin layer chromatography (A-TLC), SiliaPlate TLC, Aluminum-Backed, Silica,  $200 \mu\text{m}$ ,  $20 \times 20 \text{ cm}$ , F 254 (SiliCycle Inc., Quebec, Canada) chromatographic plates were used. Trolox, gallic acid, DPPH (1,1-diphenyl-2-picryl-hydrazil) and ABTS [2,2'-Azino-bis(3-ethylbenzothiazoline-6-sulfonic acid) diammonium salt were purchased from Sigma Aldrich (St Louis, MO, USA).

### 2.2. Sample collection and processing

The waste samples were produced from the pericarp of fruits collected directly from an orchard of *G. mangostana*, located in the municipality of Santa Bárbara - PA/Brazil, georeferenced coordinates  $1^\circ 15' 3.88'' \text{ S}$ ;  $48^\circ 16' 36.84'' \text{ O}$ , in April 2019, with authorization for collection and transportation of botanical material granted by the Authorization and Information System in Biodiversity - SISBIO, with registration number 65490-1, and activity record of access to genetic heritage registered in the National System for the Management of Genetic Heritage and Associated Traditional Knowledge – SisGen with the number A246F9A. After collection, the fruits were screened in order to classify those that had the best characteristics in terms of color, appearance and integrity of the pericarp, resulting in 94 selected fruits. The fruits were stored in plastic trays and transported to the laboratories where they were kept in a conditioned environment ( $19 \pm 2^\circ \text{ C}$ ) for approximately 15 h before processing. The first stage followed by rinsing the fruits under running water to remove coarse dirt and microorganisms adhered to the skin. After rinsing, the fruits were kept in a bath of 0.05% commercial sodium hypochlorite solution for 20 min. Then, the fruits went through a second rinse, with sterile distilled water, to remove the residual disinfectant solution. The fruits were then

pulped and the pericarp, separated for weighing and subsequent drying. The mass of fresh pericarp (MF) was 4.99 kg. After weighing, the fresh material was dehydrated in an air circulation kiln at a temperature of  $45.0 \pm 2.5$  °C for 72 h. The dry material was subjected to grinding operation in a Willey knife mill model SL-31 (SOLAB, Piracicaba, Brazil) equipped with a 10 mesh granulometric classification and standardization sieve, then it was collected, separated into fractions, labeled, and stored in low density polyethylene plastic (LDPE) bags, colorless  $45 \times 300 \times 0.04$  mm, at room temperature of 25 °C until the extraction stage was carried out. The final mass of processed waste was 1.82 kg.

### 2.3. Extracts preparation

For the extraction of bioactive compounds, an ultrasonic bath with indirect contact was used, model USC-2800A (UNIQUE Ind. and Com. Ltda., Indaiatuba, Brazil), operating at 40 kHz, power of 130 W and temperature of  $25.0 \pm 0.5$  °C. Initially, to evaluate the extracting capacity of the solvents used, as well as the selectivity of them with the analytes ( $\alpha$ - and  $\gamma$ -mangostin), the microextraction scale was used, starting from 5 g of dry and ground waste to 50 mL of solvent. The following solvents have been tested:  $\text{CHCl}_3$ , EtOAc, EtOH and MeOH, with extraction time of 30 min. The obtained solutions were filtered and the solvents, removed under reduced pressure by using a rotary evaporator model Syncore (BÜCHI Labor Technik AG, Flawil, Switzerland). Then, the extracts were named according to the respective solvents used as extracting phase: chloroformic extract (CE), ethylacetic extract (EaE), ethanolic extract (EtE) and methanolic extract (ME).

The raw ethanolic extract (REE), submitted to fractionation by HSCCC-Prep, was produced through the same procedure used to obtain the extracts in microscale. 100 g of dry waste were used for 300 mL of EtOH; 1 batch. The dry REE mass obtained was 9.638 g.

### 2.4. Evaluation of metabolic profiles by A-TLC

For the analysis,  $50 \times 50$  mm silica gel chromatography plates and 40 mm chromatographic path were used. Individual samples of each extract were prepared at a concentration of 1 mg/mL, and aliquots of 5  $\mu\text{g}/\text{spot}$  (5  $\mu\text{L}$ ) were inoculated in 5 mm bands. Then, the chromatoplates were eluted in a glass vat by using the combination of dichloromethane and methanol 9:1 (v/v) as mobile phase. After elution, the plates were observed under the incidence of 254 nm and 365 nm UV radiation, revealing the separate constituents in the form of dark and fluorescent bands, respectively. After observation, the appropriate chromogenic reagents for detection of classes of interest were applied to the plates (Hellmut et al., 1990; Kinghorn, 1997). The determination of the  $R_f$  (retention factor) of  $\alpha$  and  $\gamma$ -mangostin was performed by the identification of both by HPLC-PDA-MS.

### 2.5. Selection of two-phase solvent system

The selection of the most suitable solvent system was guided by the study and evaluation of separation or accommodation times between the phases ( $\tau$ ), and partition coefficient values (K) and

xanthones  $\alpha$ - and  $\gamma$ -mangostin separation factor ( $\alpha$ ). Each system consisted of an organic upper phase (OP) and an aqueous lower phase (AP). The phases were prepared separately for each of the tested systems. A volume of 5 mL of each phase was transferred to a  $13 \times 100$  mm glass test tube, with screw cap, and shaken vigorously for 20 s for mutual phase saturation. After stirring, the tubes were left to stand until a clear and clean separation interface was formed. Then, 100 mg of REE were added to each of the solvent systems at equilibrium followed by vigorous manual stirring for 20 s. The tubes were then left to rest and the separation time between the phases of each system was recorded. After equilibration, 1.0  $\mu\text{L}$  aliquots from both phases of each system were injected separately in an HPLC-PDA system for determination of K and  $\alpha$  values from the absolute peaks area data corresponding to analytes in the chromatograms registered. By convention, in liquid chromatography, K value is expressed as the concentration of solute in the upper phase divided by its concentration in the lower phase ( $K_{U/L}$ );  $\alpha$  value is given by the ratio between the K values of each analyte in the same solvent system ( $\alpha = K_2/K_1$ ;  $K_2 > K_1$ ) and must be greater than 1.5 to obtain an adequate resolution. K value was calculated by the ratio between the analyte peak area in OP and the peak area in AP.

### 2.6. Prep-HSCCC separation procedure

The REE fractionation and  $\alpha$ - and  $\gamma$ -mangostin isolation were performed in a preparative high-speed countercurrent chromatograph (Prep-HSCCC), model Quattro ccc (AECS-Quikprep™, United Kingdom) equipped with three independent multilayer separation columns made of polytetrafluoroethylene (PTFE), and arranged in parallel. The separation was developed in column-1 (preparative, 3.7 mm I.D. and total volume of 358 mL) using the two-phase solvent system consisting of MeOH:H<sub>2</sub>O:EtOH:Hex:MTBE 6:3:1:6:4 (v/v). For pumping of both phases, collection and monitoring of effluent during separation, Prep-HSCCC was coupled to an Isolera One flash purification system (Biotage®, Uppsala, Sweden), equipped with a quaternary solvent manager (QSM), automated fraction collector, internal detector operating in UV range (200–400 nm), and sampling loop with maximum volumetric capacity of 12 mL. The previous saturation between the system phases was made in a separation funnel by vigorous stirring repeatedly at a temperature of 25 °C. After equilibration, the two phases were separated again in different flasks and degassed by sonication for 10 min before use. AP was used as stationary, and OP, as mobile. First, column-1 was completely filled with AP at a flow of 10 mL/min in rotation at 200 rpm. The sample was dissolved in 12 mL of an AP/OP mixture (1:1, v/v) and injected into the loop to be propelled into the column along with the stationary phase. After the column was completely filled, with AP containing the sample, OP was then eluted. The elution process of mobile phase took place in tail-head direction at an OP flow of 5 mL/min. The system rotation speed was 800 rpm and the temperature was maintained at 32 °C. The effluent was monitored at wavelengths of 254 and 320 nm. The collection volume of fractions was 8 mL/tube. OP was made up of Hex/MTBE in the ratio of 6:4 (v/v), and AP, composed of MeOH/H<sub>2</sub>O/EtOH in the ratio of 6:3:1 (v/v). After the end of separation, the rotation was stopped and the stationary phase was pushed out of the col-

umn. Its content was collected, and the volume was measured in order to calculate the retention rate of the stationary phase.

### 2.7. Analysis by HPLC-PDA

For studies of REE and fractions obtained in separation by HSCCC chemical profile, it was used a modular high-performance liquid chromatography system: *Proeminence Ultra fast liquid chromatograph* (UFLC), model LC-20A (Shimadzu, Tokyo, Japan), consisting of binary pump, DGU-20A online degasser, SIL-20A auto-sampler and auto-injector, CTO-20A thermostatic column compartment, and photodiode array detection system (PDA) SPD-M20A (Shimadzu, Tokyo, Japan). Separations occurred in a RP-18, 5  $\mu$ m, 2.0  $\times$  150 mm, model Shim-pack VP - ODS (Shimadzu, Tokyo, Japan) column, kept in an oven at 28 °C. The absorption spectra were recorded in 200–800 nm range, and the chromatograms, processed at 254 nm. The mobile phase consisted of 0.1% formic acid in water (solution A), and ACN (solvent B). The separation occurred in gradient mode, with variation of 55–85% of the solvent B amount, in the range of 0–45 min and flow of 0.189 mL/min. The Volume injected per sample was 5  $\mu$ L.

### 2.8. Analysis by HPLC-ESI-MS

The determination of molecular masses and identification of compounds present in the fractions samples collected in the separation was carried out in a mass spectrometer coupled to HPLC system, model LCMS-2010 EV (Shimadzu, Tokyo, Japan), with single-stage quadrupole analyzer and electrospray ionization source (ESI). The  $m/z$  analyzer operated in the acquisition mode of full scan of positive and negative ions, in the range of  $m/z$  200 – 800, with speed of 1000 amu/s. The ESI source operated under the following conditions: flow of nebulizer gas ( $N_2$ ) of 1.5 L/min; capillary voltage, (+) 4.5 kV, (–) 3.5 kV; heater block temperature, 200 °C; curved desolvation line temperature (CDL), 230 °C. The chromatographic operating conditions of HPLC were the same as described in section 2.7 for all samples. The acquisition and processing of data generated in the analysis by HPLC-PDA-MS was done by the workstation and data management LCMSsolution (Shimadzu, Tokyo, Japan).

### 2.9. Analysis by NMR

The  $^1H$  and  $^{13}C$  Nuclear Magnetic Resonance (NMR) spectra were acquired on a Mercury 300 spectrometer (Varian, Inc., Palo Alto, USA), operating at 300 ( $^1H$ ) and 75 MHz ( $^{13}C$ ). The samples were dissolved in deuterated chloroform ( $CDCl_3$ ) or deuterated methanol (MeOD). Chemical shifts ( $\delta$ ) were expressed having as reference the solvent internal signal  $CHCl_3$  ( $^1H$ ,  $\delta$  7.25;  $^{13}C$  77.0) or  $CH_3OH$  ( $^1H$ ,  $\delta$  3.30;  $^{13}C$ , 49.0).

## 2.10. Evaluation of in vitro antioxidant capacity

### 2.10.1. DPPH $^{\cdot}$ assay

The antioxidant capacity of fractions and patterns to sequester DPPH $^{\cdot}$  radicals was determined by the method described by Sridhar and Charles (2019), with some modifications. Assays

( $n = 3$ ) were performed with the addition of a 50  $\mu$ L aliquot of each sample solubilized in methanol in concentrations of 5, 25, 50, 100, 150 and 200  $\mu$ g/mL, in a microplate containing 150  $\mu$ L of DPPH $^{\cdot}$  solution in methanol at 60  $\mu$ g/mL and absorbance 0.866. Then, the microplates were incubated for 30 min, protected from light and at room temperature (25 °C) for later measurement of absorbance at 517 nm. Trolox and gallic acid were adopted as positive control. The antioxidant capacity of samples in the sequestration of DPPH $^{\cdot}$  radical was determined by the ratio between the absorbance decay of DPPH $^{\cdot}$  solution in the presence of the sample and the absorbance of DPPH $^{\cdot}$  solution in the absence of the sample (negative control), according to Eq. (1), and the results, expressed in  $EC_{50}$  ( $\mu$ g/mL).

### Scavenging capacity against DPPH (%)

$$= \frac{A_{control} - A_{sample}}{A_{control}} \times 100 \quad (1)$$

For comparison purposes, the antioxidant capacity of fractions was also expressed as an antioxidant activity index (AAI), calculated according to Eq. (2):

$$AAI = \frac{\text{final concentration of DPPH}^{\cdot} (\mu\text{g/mL})}{EC_{50} (\mu\text{g/mL})} \quad (2)$$

The ability to sequester DPPH $^{\cdot}$  radicals from samples and standards was expressed by the AAI value, which can be classified as poor (AAI < 0.5), moderate (0.5 < AAI < 1.0), strong (1.0 < AAI < 2.0), and very strong (AAI > 2.0) (Scherer and Godoy, 2009).

### 2.10.2. ABTS $^{\cdot+}$ assay

The antioxidant capacity of fractions and patterns in the capture of ABTS $^{\cdot+}$  radical was determined from the adaptation of the method described by Sridhar and Charles (2019). A stock solution of ABTS $^{\cdot+}$  was produced by reacting the aqueous solution of ABTS (7 mM) with 140 mM aqueous solution of Potassium persulfate in the proportion of 5 mL of ABTS to 88  $\mu$ L of potassium persulfate. After 16 h of reaction, the solution was diluted and adjusted to absorbance of  $0.510 \pm 0.01$  at 734 nm. The antioxidant capacity of the compounds was determined from concentrations of 5, 25, 50, 100, 150 and 200  $\mu$ g/mL compared to ABTS $^{\cdot+}$  radical solution. The mixture was incubated, protected from light, for 10 min and its absorbances were obtained at 734 nm. The assays were performed in triplicate and trolox and gallic acid were used as positive control. The antioxidant capacity of samples in the sequestration of ABTS $^{\cdot+}$  radical was determined by the ratio between the absorbance decay of ABTS $^{\cdot+}$  solution in the presence of the sample, and the absorbance of ABTS $^{\cdot+}$  solution, in the absence of the sample (negative control), according to Eq. (3), and the results, expressed in  $EC_{50}$  ( $\mu$ g/mL).

### Scavenging capacity against ABTS $^{\cdot+}$ (%)

$$= \frac{A_{control} - A_{sample}}{A_{control}} \times 100 \quad (3)$$

### 2.11. $EC_{50}$ determination

$EC_{50}$  values of samples and standards were estimated by using a nonlinear regression model built by graphical plotting of

inhibition percentage results in function of samples concentration logarithm. Results were subjected to statistical analysis by using GraphPad Prism® software version 8.0.1 (GraphPad Software Inc. – San Diego, CA, USA). Data were treated by non-linear regression by adopting a logistic equation with 5 parameters, and the result, plotted according to dose-response inhibition of antioxidant capacity of patterns and fractions. Data were analyzed for statistical differences between treatment groups and estimated by using the Spearman ( $r$ ) correlation. All statistical tests were performed with level significance with  $p < 0.05$ .

### 3. Results and discussion

#### 3.1. Selection of extract rich in $\alpha$ - and $\gamma$ -mangostin

The de-replication of extracts, CE, EaE, EtE and Me, was performed by A-TLC and HPLC-PDA-MS to select the one that had the highest relative concentration of the main bioactive xanthenes,  $\alpha$ - and  $\gamma$ -mangostin, targeting fractionation to the isolation of both with maximum yield without the need for pre-treatment or previous fractionation of the sample, reducing the number of steps and making the procedure simpler, faster, cleaner, and cheaper.

The extracts samples were then subjected to analysis by A-TLC and to phytochemical detection tests for the characterization and comparison of chromatographic profiles (Hellmut et al., 1990; Kinghorn, 1997). The rapid identification and structural characterization of constituents of the extract selected for fractionation was carried out by HPLC-PDA-MS and it is described in Sections 3.5 and 3.6. Fig. 1 illustrates the image of a chromatographic plate with profiles of the extracts samples, revealed under the exposure of 254 nm radiation, after the chromatography development.

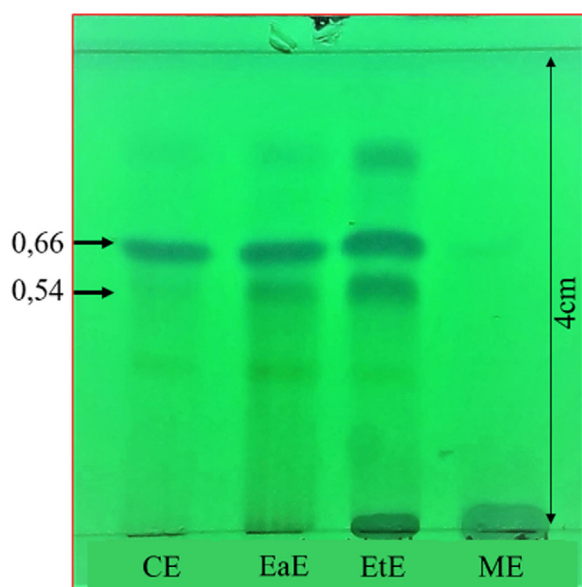


**Fig. 1** Chromatographic profiles of extracts samples on A-TLC plate exposed to 254 nm radiation; CE, chloroformic extract; EaE, ethylacetic extract; EtE, ethanolic extract; ME, methanolic extract; Retention factor ( $R_f$ ): 0.66,  $\alpha$ -mangostin; 0.54,  $\gamma$ -mangostin.

The different patterns of bands produced and detected on the plate surface (Fig. 1) reveal the differences in composition between the extracts due to the polarity degree of the solvent used as extracting phase (Suttirak and Manurakchinakorn, 2014). As can be seen in the figure (Fig. 1), the CE and ME profiles differ significantly from the other extracts. It is possible to observe in the figure (Fig. 1) that there was no migration of the ME sample applied to the plate, that is, the sample remained fully retained in the base. The lack of migration can be explained by the sample being constituted, predominantly, of molecules of high polarity and molecular weight, such as tannins and their glycosides, characterized by reactions with the appropriate detection reagents; the pattern and the number of bands observed in the CE profile shows that its composition is more complex, however, being constituted by a major substance, identified as  $\alpha$ -mangostin ( $R_f$  0.66), indicating that chloroform has a high selectivity for the removal of this component. EtOAc and EtOH solvents, according to the observed profiles of EaE and EtE (Fig. 1), can extract substances from a wide range of polarities, such as the main xanthenes and other present phenolic compounds. According to Fig. 1, EtE presented the highest metabolic diversity with a higher concentration of analytes,  $\alpha$ - ( $R_f$  0.66) and  $\gamma$ -mangostin ( $R_f$  0.54), being the extract chosen for fractionation. The choice of the appropriate solvent and the extraction method employed are crucial for obtaining natural products comprehensively and in maximized quantities, that is, matrices that are representative of the totality of metabolites present in the natural source (Hubert et al., 2017). The preliminary study of the metabolic profile carried out by A-TLC was fundamental in deciding on which of the solvents should be used in the preparation of an extract that would offer a greater metabolic diversity and a greater concentration of analytes, enabling their isolation with maximum yield.

#### 3.2. Selection and optimization of separation conditions by Prep-HSCCC

Proper separation by Prep-HSCCC depends mainly on the correct choice of a two-phase solvent system that produces values of  $0.5 < K < 2.0$  and  $\alpha > 1.5$  between analytes, with  $K$  value being the most important parameter for determining the resolution of a CCS (Friesen et al., 2015; Ito, 2005; Luo et al., 2016). Initially, two two-phase solvent systems from the “Arizona” family were tested, consisting of Hex, EtOAc, MeOH and water (HEMWat), suggested by Ito (2005) and Friesen et al. (2015) as the initial choice for a preliminary study on the polarity and solubility of analytes. Six different versions of this system, with different proportions between solvents, were tested with unsatisfactory results regarding  $K$  values for the analytes. So, four new two-phase systems, very similar in composition, were created and tested, showing better results compared to the initial system. The compositions of the systems and the respective  $K$  and  $\alpha$  values of the analytes are described in Table 1. The flow rate of the mobile phase and the speed of revolution of the coil set are two important parameters for obtaining peaks with good resolution. The flow rate delimits the separation time and the amount of stationary phase retained in the column; low speeds of rotation decrease the retention rate and very high speeds produce a widening of the peaks due to system vibration as a result of violent pulsa-

**Table 1** Partition coefficients (K) and separation factors ( $\alpha$ ) of  $\alpha$ - and  $\gamma$ -mangostin.

Two-phase solvent system: MeOH:H <sub>2</sub> O:EtOH:Hex:X:EtOAc		Partition coefficients (K)		Separation factors ( $\alpha$ )
		$\gamma$ -mangostin K <sub>1</sub>	$\alpha$ -mangostin K <sub>2</sub>	
1	6:3:1:6:3:1	1.08	4.44	4.11
2	6:3:1:6:4:0	0.48	3.12	6.50
3	6:3:1:6:3:1	0.31	1.07	3.47
4	6:3:1:6:4:0	0.77	2.07	2.69

X = Diethyl ether in 1 and 2; MTBE in 3 and 4.

tion in the column generated by high pressure (Ito, 2005). The flow of mobile phase and the speed of revolution adopted in this work were adjusted within the range of values suggested by Ito (2005) as the most usual practiced in separations in multilayer coil systems with separation preparatory columns: 5–6 mL/min; 600–800 rpm. Another important factor in obtaining a good resolution and achieving an efficient separation is the retention rate of the stationary phase in the column, which will be greater the shorter the separation or accommodation time between the two phases in the test tube. For all systems shown in Table 1, the separation time between the phases was between 10 and 20 s, that is, within the recommended limit for a satisfactory retention rate, above 50% (Ito, 2005). However, still in the testing phase in test tubes, in systems 1 and 2, the formation of precipitates was observed. This phenomenon can be explained by the high volatility of diethyl ether, which is lost continuously by vaporization at room temperature ( $25 \pm 2$  °C). The formation of precipitates promotes a constant change in the composition of these systems due to the loss of some components that become insoluble and leave the solution due to precipitation, causing compromised separation efficiency due to loss of resolution, decrease in retention rate and lack of repeatability (Ito, 2005; Luo et al., 2016; Shan and Zhang, 2010). Diethyl ether was then replaced by MTBE, thus, solving the problem of volatility and making the system more stable. According to results shown in Table 1, system 4 presented satisfactory K and  $\alpha$  values for production of efficient separation, being the system chosen for isolation of  $\alpha$ - and  $\gamma$ -mangostin by HSCCC. The effect of different amounts of sample loading on the separation efficiency was also evaluated. The introduction of large amounts of sample in the system can lead to large losses in the stationary phase and compromise the resolution of peaks related to analytes, especially those with small K values. However, the injection of small amounts of sample may reduce the yield of products (Friesen et al., 2015; Ito, 2005; Li et al., 2017). Samples were injected with 250, 450 and 650 mg of REE, dissolved in 12 mL of a two phases mixture (1:1, v/v), and results produced were evaluated. The chromatographic separation of sample with 650 mg of REE presented a resolution of peaks, referring to analytes, very similar to those obtained for other two quantities of samples investigated, however, its yield was significantly higher with a small decrease in the retention rate of stationary phase, about 5%.

Results obtained in the study of selection and optimization of experimental conditions of operational parameters of separation by HSCCC were used in the fractionation of REE for analytes isolation. Therefore, experimental conditions practiced in the separation were as follows: solvent system composed of MeOH:H<sub>2</sub>O:EtOH:Hex:MTBE 6:3:1:6:4 (v/v);

tail-head elution direction (normal phase); revolution speed of 800 rpm; mobile phase flow of 5 mL/min; loading of 650 mg of REE sample.

### 3.3. Fractionation of REE by Prep-HSCCC

Phenolic constituents of REE were separated by Prep-HSCCC, in a single step, in 35 min range. The fractionation of 650 mg of REE initially produced 195 fractions. The fractions were monitored by A-TLC for the identification and assembly of those with similar chemical profiles. The assembly procedure resulted in only four fractions, referred to as F1, F2, F3 and F4. The fractionation chromatogram of REE by Prep-HSCCC is shown in Fig. 2. The blue trace observed in the chromatogram (Fig. 2), which delimits the area between 12 and 70 min, indicates the elution time of mobile phase. F1 and F2 fractions were produced between 12 and 20 min elution range. Peaks identified as F3, pink region; and F4, green region, were registered between 20 and 47 min and correspond to the 3 and 4 resulting fractions, respectively. It was observed that the mass quantity obtained for each fraction in this separation was 55.2 mg of F1; 56.3 mg of F2; 222.6 mg of F3; and 65.1 mg of F4. The method achieved a recovery above 61%, and the total separation yield was 399.2 mg.

### 3.4. Prep-HSCCC system accuracy

The accuracy of chromatographic system for REE fractionation and xanthenes isolation was tested by successive injection of sample on five consecutive days. The relative standard deviation (RSD) for mass values of fractions F1 to F4, obtained in the five injections were 5.2%, 6.5%, 3.8% and 4.5%, respectively.

### 3.5. Characterization of REE and fractions chromatographic profile

The characterization of REE and fractions metabolic profile was done through samples analysis by HPLC-PDA-MS. Compounds referring to peaks, numbered from 1 to 9, in REE chromatogram (Fig. 3, A), are listed in Table 2 with their respective retention times ( $t_R$ ), spectral data of maximum absorption in UV-Vis ( $\lambda_{max}$ ) and protonated ( $[M + H]^+$ ) and deprotonated ( $[M - H]^-$ ) molecules.

The identity of each detected compound was determined by comparing instrumental data generated in the analysis with data already reported in literature for GML xanthenes (Fang et al., 2011; Shan and Zhang, 2010; Walker, 2007; Wittenauer et al., 2012). The elution order of detected species,

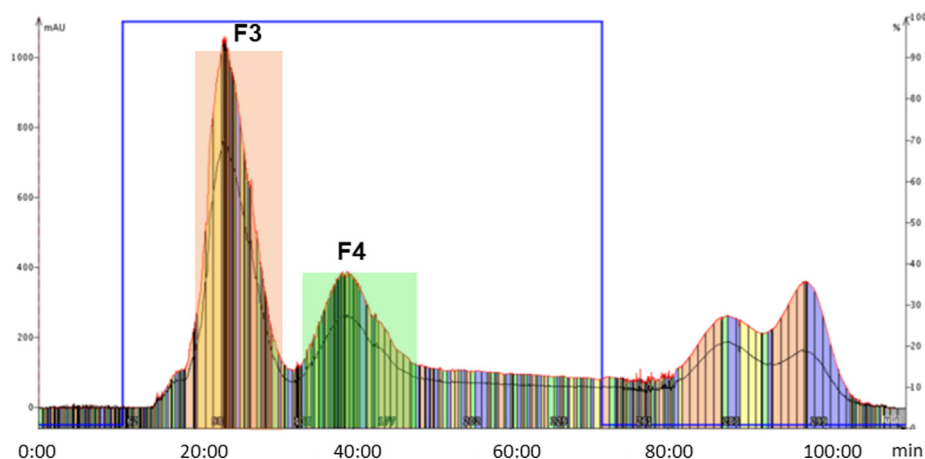


**Fig. 2** Chromatograms for Raw Ethanolic Extract (REE) fractionation by HSCCC: red line (254 nm); black line: (320 nm); solvent system: MeOH:H<sub>2</sub>O:EtOH:Hex:MTBE (6:3:1:6:4, v/v); rotation speed: 800 rpm; flow: 5 mL/min; sample mass: 650 mg; stationary phase retention: 80%; F3:  $\alpha$ -mangostin; F4:  $\gamma$ -mangostin.

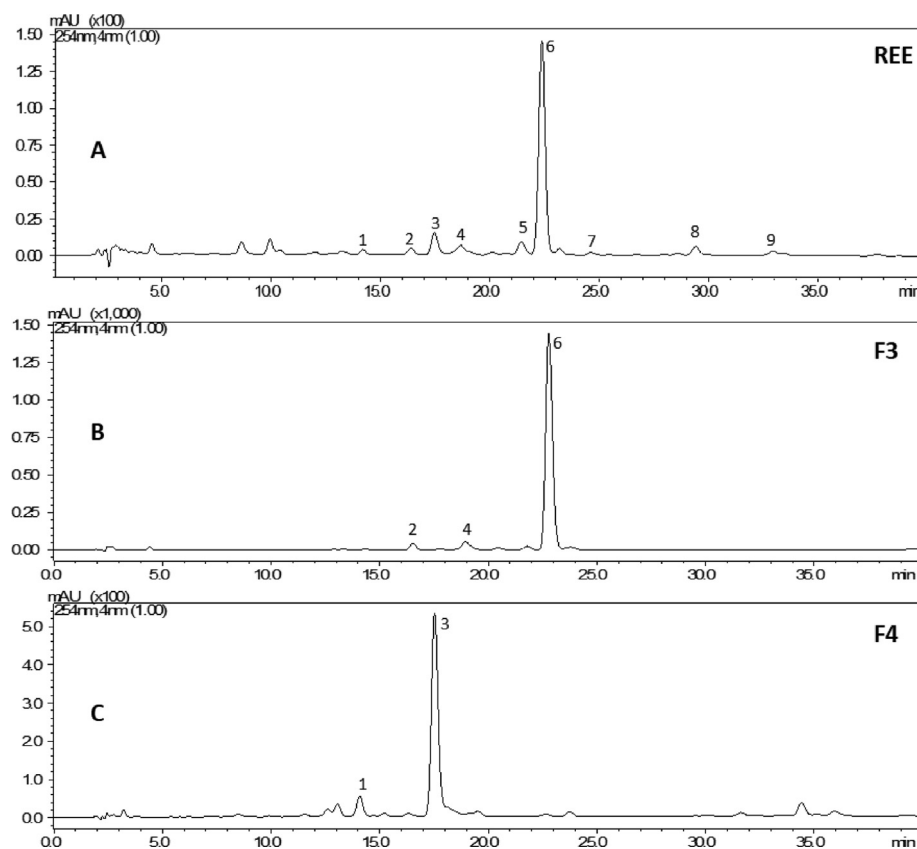


**Fig. 3** Chromatograms by HPLC-PDA processed at 254 nm: (A) raw ethanolic extract (REE); (B) fraction F3,  $\alpha$ -mangostin with purity above 96%; (C) fraction F4,  $\gamma$ -mangostin with purity above 93%.

recorded by the peaks in REE chromatogram (Fig. 3, A), also contributed to the identities confirmation. The elution order was exactly the same as that observed in other studies involving studies of characterization and separation of xanthenes from GML by HPLC that used reverse phase column (RP-18) and mobile phase composed of acidified water/ACN (Aisha et al., 2012; Fang et al., 2011; Muchtaridi et al., 2017; Shan and Zhang, 2010; Walker, 2007; Wittenauer et al.,

2012). The structures of xanthenes identified in REE are shown in Fig. 4.

Results obtained and summarized in Table 2 confirmed the identities of  $\alpha$ -mangostin as the most abundant species present in F3, referring to peak 6 (Fig. 3, B), with 96.3% purity; and  $\gamma$ -mangostin, present in F4, referring to peak 3 (Fig. 3, C), with 93.2% purity. Purities were calculated by normalization of peak areas corresponding to substances in the chromatograms

**Table 2** Retention time data ( $t_R$ ), absorption spectra of UV–Vis and  $m/z$  of xanthenes detected in *Garcinia mangostana* pericarp raw ethanolic extract by HPLC-PDA-MS.

Compound	$t_R$ (min)	Xanthone	$\lambda_{\max}$ (nm)*	$[M+H]^+ / [M-H]^- (m/z)$	LC-ESI(-) – MS: $m/z$ (intensity rel. %)
1	14.11	Mangostanol	257/317/486/ 423	427/425	[427](100), 409(15)
2	16.73	1,7-dihydroxy-3-methoxy-2-prenylxanthone	256/311/657/ 481	327/325	[327](100), 271(25)
3	17.66	$\gamma$ -mangostin	243/259/317/ 363	397/395	[397](100), 341(10)
4	19.02	8-Deoxigartanin	245/258/320/ 366	381/379	[381](100), 325(10), 269(7)
5	21.78	Gartanin	258/282/347	397/395	[397](100), 341(32), 285(18)
6	22.81	$\alpha$ -Mangostin	244/316/657	411/409	[411](100), 355(12)
7	25.36	Garcinone E	225/259/320/ 362	465/463	[465](100), 439(5), 409(9)
8	30.04	9-Hydroxycabalaxanthone	244/288/330	409/407	[409](100), 383(12), 353(6)
9	33.74	$\beta$ -Mangostin	245/258/316/ 345	425/423	[425](100), 399(10), 369(5)

\* Note: UV–Vis absorption spectra of compounds were registered in mobile phase consisting of: 0,1% formic acid in water (solution A); ACN (solvent B).

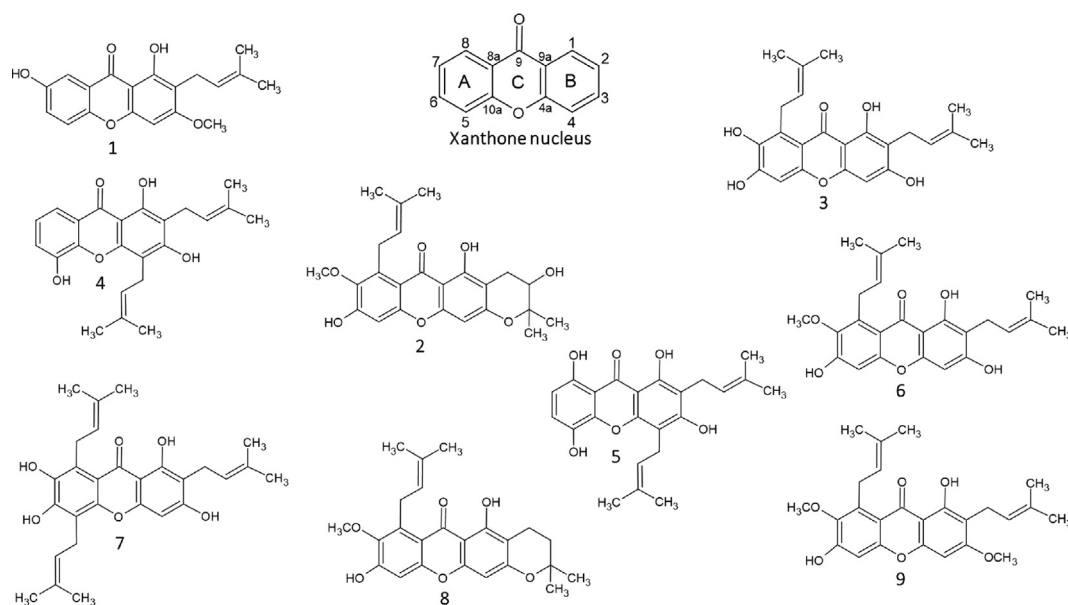


**Fig. 4** Structures of xanthenes identified in the *Garcinia mangostana* L. pericarp raw ethanolic extract by LC-PDA-MS: **xanthone nucleus**; Mangostanol, **1**; 1,7- dihydroxy-3-methoxy-2-prenylxanthone, **2**;  $\gamma$ -mangostin, **3**; 8-Deoxigartanin, **4**; Gartanin, **5**;  $\alpha$ -mangostin, **6**; Garcinone E, **7**; 9- Hydroxycabalaxanthone, **8**;  $\beta$ -mangostin, **9**.

and are expressed as percentages of relative area. These results demonstrate the high resolution power of HSCCC and the efficiency of the method that was able to promote the isolation of analytes in just under 35 min, reaching levels of purity very close to those obtained in other works of CCS reported in the most recent literature (Fang et al., 2011; Michel et al., 2012; Shan and Zhang, 2010). The chromatograms of F1 and F2 fractions are shown in Fig. S1A (section S1, supplementary material). Results of F1 analysis (Fig. S1A, D) showed that 9-hydroxycabalaxanthone and  $\beta$ -mangostin, peaks 8 and 9, respectively, are present in predominant quantities, corresponding to 38.7 and 25.0% of the total in mass, respectively. These molecules have very similar structures and low

degrees of polarity, which is why they were the first to be eluted by the organic mobile phase in tail-head elution mode (Shan and Zhang, 2010). The profile of F2 (Fig. S1A, E) shows that it is mainly composed of a mixture of two major constituents, gartanin and  $\alpha$ -mangostin, corresponding to 13.8% and 55.1% by mass, peaks 5 and 6, respectively. In REE chromatogram, peaks 3 and 6, referring to  $\alpha$ - and  $\gamma$ -mangostin, have relative percentage areas of 12.3 and 48.9%, respectively.

### 3.6. Structural identification of $\alpha$ - and $\gamma$ -mangostin

The structural determination of the isolated substance in F3 was performed from ESI-MS,  $^1H$  and  $^{13}C$  NMR spectral data

generated in the analysis and by comparison with data registered in the literature (Fang et al., 2011; Michel et al., 2012). The ESI-MS data for the substance referring to peak 6, in the F3 chromatogram, are  $m/z$  411  $[M + H]^+$  (100), 409  $[M - H]^-$  (100); NMR  $^1H$  ( $CDCl_3$ , 300 MHz)  $\delta$ : 1.62, 1.63 (3H each, s, H-4' e H-4''), 1.75 (3H, s, H-5'), 1.83 (3H, s, H-5''), 3.44 (2H, d,  $J = 7.2$  Hz, H-1'), 3.80 (3H, s,  $OCH_3$ ), 4.09 (2H, d,  $J = 6.0$  Hz, H-1''), 5.28 (2H, m, H-2' e H-2''), 6.27 (1H, s, H-4), 6.80 (1H, s, H-5), 13.75 (1H, s, C-1-OH);  $^{13}C$  NMR ( $CDCl_3$ , 75 MHz)  $\delta$ : 17.90 (C-5''), 18.20 (C-5'), 21.42 (C-1'), 25.80 (C-4''), 25.83 (C-4'), 26.55 (C-1''), 62.03 ( $OCH_3$ ), 93.27 (C-4), 101.54 (C-5), 103.60 (C-9a), 108.43 (C-2), 112.16 (C-8a), 121.43 (C-2'), 123.12 (C-2''), 132.15 (C-3''), 135.75 (C-3'), 137.02 (C-8), 142.53 (C-7), 154.52 (C-4a), 155.05 (C-6), 155.76 (C-10a), 160.59 (C-1), 161.61 (C-3), 182.02 (C-9).  $^1H$  NMR and  $^{13}C$  NMR spectral data coincided with data in the literature, confirming that the substance isolated in F3 was  $\alpha$ -mangostin. The identity of the compound isolated in F4 was determined from its spectral data from ESI-MS,  $^1H$  NMR and  $^{13}C$  NMR. ESI-MS data are  $m/z$  397  $[M + H]^+$  (100), 395  $[M - H]^-$  (100);  $^1H$  NMR (Methanol- $D_4$ , 300 MHz)  $\delta$ : 1.64, 1.66 (3H each, s, H-4' e H-4''), 1.77 (3H, s, H-5'), 1.82 (3H, s, H-5''), 3.32 (2H, d,  $J = 7.2$  Hz, H-1'), 4.16 (2H, d,  $J = 6.0$  Hz, H-1''), 5.27 (2H, m, H-2' e H-2''), 6.38 (1H, s, H-4), 6.80 (1H, s, H-5), 13.92 (1H, s, C-1-OH).  $^{13}C$  NMR (Methanol- $D_4$ , 75 MHz)  $\delta$ : 17.20 (C-5''), 17.92 (C-5'), 21.30 (C-1'), 25.26 (C-4''), 25.40 (C-4'), 26.20 (C-1''), 92.20 (C-4), 100.30 (C-5), 102.60 (C-9a), 110.2 (C-2), 111.3 (C-8a), 122.90 (C-2'), 123.90 (C-2''), 130.6 (C-3'), 130.8 (C-3''), 143.5 (C-7), 153.60 (C-4a), 154.80 (C-6), 155.70 (C-10a), 161.0 (C-1), 162.0 (C-3), 182.4 (C-9). NMR data are in agreement with data registered in other works in the literature (Fang et al., 2011; Michel et al., 2012), confirming that the compound isolated in F4 is  $\gamma$ -mangostin.

### 3.7. Antioxidant potential of the fractions obtained

$EC_{50}$  results that represent the antioxidant potential of fractions and patterns in the capture of DPPH $\cdot$  and ABTS $\cdot^+$  radicals are shown in Table 3. When evaluating the ability to sequester DPPH $\cdot$  radicals, the results obtained for F2 and F4 stand out, with  $EC_{50}$  of 8.42 and 8.43  $\mu\text{g/mL}$ , respectively. By comparing the results, it is possible to conclude that F2 and F4 have the capacity to scavenge DPPH $\cdot$  radicals almost nine times greater than the measured capacity for F3, and three times greater than F1. The variation in the antioxidant capacity of fractions can be attributed to the profile of mangostin present in majority quantities, corroborating the existence of a high correlation between the chemical structure and the activity of these xanthenes (Scherer and Godoy, 2009; Suttirak and Manurakchinakorn, 2014; Thong et al., 2015). As for the low antioxidant capacity exhibited by F3 compared to DPPH $\cdot$  radical, Tjahjani et al. (2014) reported a similar result of  $EC_{50}$  for  $\alpha$ -mangostin. In comparison with  $EC_{50}$  values obtained for different pericarp extracts, prepared by using different solvents as extracting phase,  $\alpha$ -mangostin exhibited a low antioxidant capacity, however, when measured by means of other activity assays, such as Superoxide Dismutase (SOD) and Total Antioxidant Status (TAS), it exhibited greater activity than the extracts studied. This effect suggests that  $\alpha$ -mangostin can act as an antioxidant through another

**Table 3** Antioxidant capabilities of F1, F2, F3 and F4 patterns and fractions, via sequestration of DPPH $\cdot$  and ABTS $\cdot^+$  radicals.

Sample	DPPH $\cdot$ ( $EC_{50}$ $\mu\text{g/mL}$ )	ABTS $\cdot^+$ ( $EC_{50}$ $\mu\text{g/mL}$ )
Gallic Acid	1,70 $\pm$ 1,03;a	1,15 $\pm$ 0,92;a
Trolox	7,15 $\pm$ 1,09;b	2,63 $\pm$ 1,20;b
F1	25,63 $\pm$ 1,62;c,d	11,46 $\pm$ 2,54;c,d
F2	8,42 $\pm$ 1,32;d,b	4,54 $\pm$ 1,58;a,b
F3	71,10 $\pm$ 1,14;e,f	29,33 $\pm$ 0,90;e,f
F4	8,43 $\pm$ 0,65;g,b	3,31 $\pm$ 1,45;a,b

\*Note: Values were expressed by the concentration required for decay of 50% of free radicals; All experiments presented significance with  $p < 0.05$ . According to Tukey test, different letters present significant differences when comparing the fractions with reference standards.

mechanism besides the transfer of hydrogen atoms (HAT) (Tjahjani et al., 2014). The reduction of a hydroxyl group (OH) in  $\alpha$ -mangostin is the main factor responsible for decreasing the capacity of HAT in relation to the activities of  $\gamma$ -mangostin and gartanine, which have the same number of OH groups in the two rings, however, in the gartanine, the prenyl groups are together in ring B (Fig. 4), decreasing the steric impediment on the OH groups in ring A, in addition to favoring HAT, since these groups are p-substituted in this ring, which decreases the strength of the O-H bond and contributes to the formation of a stable intermediate radical by displacement of the unpaired electron (Suttirak and Manurakchinakorn, 2014). Due to the lack of standardization in procedures for evaluating the antioxidant capacity of extracts and pure compounds by using DPPH $\cdot$  method, and due to the dependence of inhibition activity and  $EC_{50}$  values on the final concentration of the radical, the activities expressed in AAI values allow an result evaluation more accurate, in terms of comparison (Scherer and Godoy, 2009; Sridhar and Charles, 2019). The final concentration of DPPH solution after adding the samples was 45.0  $\mu\text{g/mL}$ . Calculated AAI values for gallic acid and fractions, F1, F2, F3 and F4, were 26.47, 1.75, 5.34, 0.63 and 5.33, respectively. The AAI value calculated for gallic acid coincided with the value obtained by Scherer and Godoy (2009). In this work, authors proposed a scale for classifying the antioxidant power of samples tested by DPPH $\cdot$  method based on the AAI value. The AAI value for F3 fraction indicates that it exhibited moderate activity; F1 fraction exhibited strong activity; and fractions F2 and F4 have very strong activity.

Figure S2 (Section S1, supplementary material) presents graphs of the inhibition activity (%) of DPPH $\cdot$  (a) and ABTS $\cdot^+$  (b) radicals in function of samples concentration ( $\mu\text{g/mL}$ ).

The fractions collected and the tested patterns showed greater antioxidant efficiency in the ABTS $\cdot^+$  radical sequestration, with lower  $EC_{50}$  values, when compared with values found for capture of DPPH $\cdot$  radical. (Table 3) However, it is observed that the relative differences between the activity values for samples and standards remained constant. Again, the sequestering capacity of F2 and F4 stands out, with  $EC_{50}$  values of 4.54 and 3.31  $\mu\text{g/mL}$ , respectively. The discrepancy observed between the results can be explained in part by the use of different methods to estimate the antioxidant capacity of the fraction samples, by the differences in the performance

of the procedure and the use of different reagents in each method (Villaño et al., 2006). However, although both assays are based on electron transfer mechanisms between antioxidant compounds and radicals, according to Sridhar and Charles (2019), the differences in the stereochemistry of ABTS<sup>•+</sup> and DPPH<sup>•</sup> radicals, as well as the solubility, polarity and metal-chelating capacity of these compounds may affect the results and generate the observed differences. The antioxidant activity tests demonstrated the pharmacological, economic and technological potential of fractions obtained from GML waste. Patterns of  $\alpha$ - and  $\gamma$ -mangostin, with purity levels close to those obtained in this work are sold on market at average prices of USD 30.0/mg. The use of mangosteen waste for the extraction and obtaining of organic molecules with useful properties in combating effects of oxidative stress and related diseases, such as premature aging, diabetes, cancer and other associated diseases, fits into new technologies for minimizing environmental impact with prospects for generation of new molecules with noble applications.

#### 4. Conclusion

The countercurrent separation method proposed in this work proved to be highly efficient in the isolation and purification of mangostins present in predominant quantities in the GML pericarp extract. The strategies adopted for preparation and de-replication of the extract have a connotation of green chemistry, and contributed to make the procedure simpler, faster, cheaper and more efficient, favoring the obtaining of an extract rich in  $\alpha$  and  $\gamma$ -mangostin and their isolations with high yields and purities in one step.

The obtaining of metabolic concentrates through the strategy used by CCC followed by the investigation of antioxidant capacity demonstrated the biological potential of substances present in its concentrates and that the strategically planned method can generate products with a high degree of purity aimed at economic sectors. The simplicity of the procedure and the yields obtained will allow cheaper costs and access to enough of these standards for various biological assays and the elaboration of products with high value-added.

In this work, the integration of extraction, isolation, monitoring, identification, and biological assays activities techniques is highlighted as technical-scientific guidelines for obtaining metabolic concentrates with high purity and high economic impact, as well as the substances that showed potential for biological activity, relatively equal to or greater than those that already exist in the market and that can be transformed into a product with commercialization potential perspective. In this sense, the development of this process from an agro-industrial waste will certainly have an impact on the use and generation of a noble product on a preparative scale.

#### Declaration of Competing Interest

The authors declare that they have no known competing financial interests or personal relationships that could have appeared to influence the work reported in this paper.

#### Acknowledgements

The authors would like to thank CAPES and PROPESP/UFPA for granting a scholarship and financial support.

#### Appendix A. Supplementary material

Supplementary data to this article can be found online at <https://doi.org/10.1016/j.arabjc.2021.103252>.

#### References

- Aisha, A.F.A., Abu-Salah, K.M., Siddiqui, M.J., Ismail, Z., Majid, A. M.S.A., 2012. Quantification of  $\alpha$ -,  $\beta$ - and  $\gamma$ -mangostin in *Garcinia mangostana* fruit rind extracts by a reverse phase high performance liquid chromatography. *J. Med. Plants Res.* 6, 4526–4534. <https://doi.org/10.5897/JMPR11.1253>.
- Aizat, W.M., Ahmad-Hashim, F.H., Syed Jaafar, S.N., 2019a. Valorization of mangosteen, “The Queen of Fruits”, and new advances in postharvest and in food and engineering applications: a review. *J. Adv. Res.* 20, 61–70. <https://doi.org/10.1016/j.jare.2019.05.005>.
- Aizat, W.M., Jamil, I.N., Ahmad-Hashim, F.H., Noor, N.M., 2019b. Recent updates on metabolite composition and medicinal benefits of mangosteen plant. *PeerJ* 7, <https://doi.org/10.7717/peerj.6324> e6324.
- Altendorf, S., 2018. Mainstreaming a niche market 9.
- Ashton, M.M., Dean, O.M., Walker, A.J., Bortolasci, C.C., Ng, C.H., Hopwood, M., Harvey, B.H., Möller, M., McGrath, J.J., Marx, W., Turner, A., Dodd, S., Scott, J.G., Khoo, J.-P., Walder, K., Sarris, J., Berk, M., 2019. The Therapeutic Potential of Mangosteen Pericarp as an Adjunctive Therapy for Bipolar Disorder and Schizophrenia. *Front. Psychiatry* 10. <https://doi.org/10.3389/fpsy.2019.00115>.
- de Carvalho, J.E.U., 2014. Mangostanzeiro: botânica, propagação, cultivo e utilização. *Rev. Bras. Frutic.* 36, 148–155. <https://doi.org/10.1590/0100-2945-454/13>.
- Chen, G., Li, Y., Wang, W., Deng, L., 2018. Bioactivity and pharmacological properties of  $\alpha$ -mangostin from the mangosteen fruit: a review. *Expert Opin. Ther. Pat.* 28, 415–427. <https://doi.org/10.1080/13543776.2018.1455829>.
- Cheok, C.Y., Mohd Adzahan, N., Abdul Rahman, R., Zainal Abedin, N.H., Hussain, N., Sulaiman, R., Chong, G.H., 2018. Current trends of tropical fruit waste utilization. *Crit. Rev. Food Sci. Nutr.* 58, 335–361. <https://doi.org/10.1080/10408398.2016.1176009>.
- Chisté, R.C., Faria, L.J.G. de, Lopes, A.S., Mattietto, R. de A., 2009. Características físicas e físico-química da casca de mangostão em três períodos da safra. *Rev. Bras. Frutic.* 31, 416–422. <https://doi.org/10.1590/S0100-29452009000200015>.
- Cui, J., Hu, W., Cai, Z., Liu, Y., Li, S., Tao, W., Xiang, H., 2010. New medicinal properties of mangostins: analgesic activity and pharmacological characterization of active ingredients from the fruit hull of *Garcinia mangostana* L. *Pharmacol. Biochem. Behav.* 95, 166–172. <https://doi.org/10.1016/j.pbb.2009.12.021>.
- EL-Kenawy, A.E.-M., Hassan, S.M.A., Osman, H.-E.H., 2019. Chapter 3.29 - Mangosteen (*Garcinia mangostana* L.). In: Nabavi, S.M., Silva, A.S. (Eds.), *Nonvitamin and Nonmineral Nutritional Supplements*. Academic Press, pp. 313–319. <https://doi.org/10.1016/B978-0-12-812491-8.00045-X>.
- Fang, L., Liu, Y., Zhuang, H., Liu, W., Wang, X., Huang, L., 2011. Combined microwave-assisted extraction and high-speed countercurrent chromatography for separation and purification of xanthenes from *Garcinia mangostana*. *J. Chromatogr. B* 879, 3023–3027. <https://doi.org/10.1016/j.jchromb.2011.08.040>.
- FAO, 2019. The state of food and agriculture 2019. Moving forward on food lost and waste reduction. Rome.
- Fierascu, R.C., Fierascu, I., Avramescu, S.M., Sieniawska, E., 2019. Recovery of natural antioxidants from agro-industrial side streams through advanced extraction techniques. *Molecules* 24. <https://doi.org/10.3390/molecules24234212>.
- Filho, W.B. do N., Franco, C.R., 2015. Avaliação do Potencial dos Resíduos Produzidos Através do Processamento Agroindustrial no Brasil. *Rev. Virtual Quím.* 7, 1968–1987. <https://doi.org/10.5935/1984-6835.20150116>.
- Friesen, J.B., McAlpine, J.B., Chen, S.-N., Pauli, G.F., 2015. Countercurrent separation of natural products: an update. *J. Nat. Prod.* 78, 1765–1796. <https://doi.org/10.1021/np501065h>.

- Hellmut, Jork, Funk, Werner, Fischer, Walter, Wimmer, Hans, 1990. *Thin-Layer Chromatography: Reagents and Detection Methods*, 1a. ed. New York.
- Hubert, J., Nuzillard, J.-M., Renault, J.-H., 2017. Dereplication strategies in natural product research: How many tools and methodologies behind the same concept?. *Phytochem. Rev.* 16, 55–95. <https://doi.org/10.1007/s11101-015-9448-7>.
- Ibrahim, M.Y., Hashim, N.M., Mariod, A.A., Mohan, S., Abdulla, M. A., Abdelwahab, S.I., Arbab, I.A., 2016.  $\alpha$ -Mangostin from *Garcinia mangostana* Linn: an updated review of its pharmacological properties. *Arab. J. Chem.* 9, 317–329. <https://doi.org/10.1016/j.arabjc.2014.02.011>.
- Ito, Y., 2005. Golden rules and pitfalls in selecting optimum conditions for high-speed counter-current chromatography. *J. Chromatogr. A* 1065, 145–168. <https://doi.org/10.1016/j.chroma.2004.12.044>.
- Jaisin, Y., Ratanachamnong, P., Kuanpradit, C., Khumpum, W., Suksamrarn, S., 2018. Protective effects of  $\gamma$ -mangostin on 6-OHDA-induced toxicity in SH-SY5Y cells. *Neurosci. Lett.* 665, 229–235. <https://doi.org/10.1016/j.neulet.2017.11.059>.
- Ketsa, S., Paull, R.E., 2011. 1 - Mangosteen (*Garcinia mangostana* L.). In: Yahia, E.M. (Ed.), *Postharvest Biology and Technology of Tropical and Subtropical Fruits*, Woodhead Publishing Series in Food Science, Technology and Nutrition. Woodhead Publishing, pp. 1–32e. <https://doi.org/10.1533/9780857092618.1>.
- Kinghorn, A.D., 1997. *Plant Drug Analysis. A Thin Layer Chromatography Atlas*. Second Edition By H. Wagner and S. Bladt (Universität München). Photographs by V. Rickl. Springer-Verlag, Brooklyn, New York. 1996. xv + 384 pp. 19.5 × 24 cm. \$198.00. ISBN 3-540-58676-8. *J. Nat. Prod.* 60, 428–428. <https://doi.org/10.1021/np960627o>.
- Lee, H.N., Jang, H.Y., Kim, H.J., Shin, S.A., Choo, G.S., Park, Y.S., Kim, S.K., Jung, J.Y., 2016. Antitumor and apoptosis-inducing effects of  $\alpha$ -mangostin extracted from the pericarp of the mangosteen fruit (*Garcinia mangostana* L.) in YD-15 tongue mucocarcinoma cells. *Int. J. Mol. Med.* 37, 939–948. <https://doi.org/10.3892/ijmm.2016.2517>.
- Leyva-López, N., Lizárraga-Velázquez, C.E., Hernández, C., Sánchez-Gutiérrez, E.Y., 2020. Exploitation of agro-industrial waste as potential source of bioactive compounds for aquaculture. *Foods* 9, 843. <https://doi.org/10.3390/foods9070843>.
- Li, K., Wu, L., Chen, Y., Li, Y., Wang, Q., Li, M., Hao, K., Zhang, W., Jiang, S., Wang, Z., 2020. Cytotoxic and antiproliferative effects of  $\beta$ -mangostin on Rat C6 glioma cells depend on oxidative stress induction via PI3K/AKT/mTOR pathway inhibition. *Drug Des. Devel. Ther.* 14, 5315–5324. <https://doi.org/10.2147/DDDT.S278414>.
- Li, Y., Li, L., Cui, Y., Zhang, S., Sun, B., 2017. Separation and purification of polyphenols from red wine extracts using high speed counter current chromatography. *J. Chromatogr. B* 1054, 105–113. <https://doi.org/10.1016/j.jchromb.2017.03.006>.
- Luo, L., Cui, Y., Zhang, S., Li, L., Li, Y., Zhou, P., Sun, B., 2016. Preparative separation of grape skin polyphenols by high-speed counter-current chromatography. *Food Chem.* 212, 712–721. <https://doi.org/10.1016/j.foodchem.2016.06.009>.
- Marzaimi, I.N., Aizat, W.M., 2019. Chapter 17 - Current review on mangosteen usages in antiinflammation and other related disorders. In: Watson, R.R., Preedy, V.R. (Eds.), *Bioactive Food as Dietary Interventions for Arthritis and Related Inflammatory Diseases* (Second Edition). Academic Press, pp. 273–289. <https://doi.org/10.1016/B978-0-12-813820-5.00017-9>.
- Michel, T., Destandau, E., Fougère, L., Elfakir, C., 2012. New “hyphenated” CPC-HPLC-DAD-MS strategy for simultaneous isolation, analysis and identification of phytochemicals: application to xanthenes from *Garcinia mangostana*. *Anal. Bioanal. Chem.* 404, 2963–2972. <https://doi.org/10.1007/s00216-012-6430-8>.
- Muchtaridi, M., Puteri, N.A., Milanda, T., Musfiroh, I., 2017. Validation analysis methods of  $\alpha$ -mangostin,  $\gamma$ -mangostin and gartanin mixture in mangosteen (*Garcinia mangostana* L.) fruit rind extract from West Java with HPLC. *J. Appl. Pharm. Sci.* 7, 125–130.
- Ovalle-Magallanes, B., Eugenio-Pérez, D., Pedraza-Chaverri, J., 2017. Medicinal properties of mangosteen (*Garcinia mangostana* L.): a comprehensive update. *Food Chem. Toxicol.* 109, 102–122. <https://doi.org/10.1016/j.fct.2017.08.021>.
- Sacramento, C.K. do, Coelho Júnior, E., Carvalho, J.E.U. de, Müller, C.H., Nascimento, W.M.O. do, 2007. Cultivo do mangostão no Brasil. *Rev. Bras. Frutic.* 29, 195–203. <https://doi.org/10.1590/S0100-29452007000100042>.
- Sagar, N.A., Pareek, S., Sharma, S., Yahia, E.M., Lobo, M.G., 2018. Fruit and vegetable waste: bioactive compounds, their extraction, and possible utilization. *Compr. Rev. Food Sci. Food Saf.* 17, 512–531. <https://doi.org/10.1111/1541-4337.12330>.
- Scherer, R., Godoy, H.T., 2009. Antioxidant activity index (AAI) by the 2,2-diphenyl-1-picrylhydrazyl method. *Food Chem.* 112, 654–658. <https://doi.org/10.1016/j.foodchem.2008.06.026>.
- Shan, Y., Zhang, W., 2010. Preparative separation of major xanthenes from mangosteen pericarp using high-performance centrifugal partition chromatography. *J. Sep. Sci.* 33, 1274–1278. <https://doi.org/10.1002/jssc.200900774>.
- Shandiz, H.T., Razavi, B.M., Hosseinzadeh, H., 2017. Review of *Garcinia mangostana* and its Xanthenes in metabolic syndrome and related complications. *Phytother. Res.* 31, 1173–1182. <https://doi.org/10.1002/ptr.5862>.
- Shibata, M.-A., Harada-Shiba, M., Shibata, E., Tosa, H., Matoba, Y., Hamaoka, H., Iinuma, M., Kondo, Y., 2019. Crude  $\alpha$ -mangostin suppresses the development of atherosclerotic lesions in apoE-deficient mice by a possible M2 macrophage-mediated mechanism. *Int. J. Mol. Sci.* 20. <https://doi.org/10.3390/ijms20071722>.
- Shibata, M.-A., Iinuma, M., Morimoto, J., Kurose, H., Akamatsu, K., Okuno, Y., Akao, Y., Otsuki, Y., 2011.  $\alpha$ -Mangostin extracted from the pericarp of the mangosteen (*Garcinia mangostana* Linn) reduces tumor growth and lymph node metastasis in an immunocompetent xenograft model of metastatic mammary cancer carrying a p53 mutation. *BMC Med.* 9, 69. <https://doi.org/10.1186/1741-7015-9-69>.
- Sridhar, K., Charles, A.L., 2019. In vitro antioxidant activity of Kyoho grape extracts in DPPH and ABTS assays: estimation methods for EC50 using advanced statistical programs. *Food Chem.* 275, 41–49. <https://doi.org/10.1016/j.foodchem.2018.09.040>.
- Suttirak, W., Manurakchinakorn, S., 2014. In vitro antioxidant properties of mangosteen peel extract. *J. Food Sci. Technol.* 51, 3546–3558. <https://doi.org/10.1007/s13197-012-0887-5>.
- Thong, N.M., Quang, D.T., Bui, N.H.T., Dao, D.Q., Nam, P.C., 2015. Antioxidant properties of xanthenes extracted from the pericarp of *Garcinia mangostana* (Mangosteen): a theoretical study. *Chem. Phys. Lett.* 625, 30–35. <https://doi.org/10.1016/j.cplett.2015.02.033>.
- Tjahjani, S., Widowati, W., Khiong, K., Suhendra, A., Tjokropranoto, R., 2014. Antioxidant Properties of *Garcinia mangostana* L (Mangosteen) Rind. *Procedia Chem.*, International Seminar on Natural Product Medicines, ISNPM 2012 13, 198–203. <https://doi.org/10.1016/j.proche.2014.12.027>.
- Torres-León, C., Ramírez-Guzmán, N., Londoño-Hernández, L., Martínez-Medina, G.A., Díaz-Herrera, R., Navarro-Macias, V., Álvarez-Pérez, O.B., Picazo, B., Villarreal-Vázquez, M., Ascacio-Valdes, J., Aguilar, C.N., 2018. Food waste and byproducts: an opportunity to minimize malnutrition and hunger in developing countries. *Front. Sustain. Food Syst.* 2. <https://doi.org/10.3389/fsufs.2018.00052>.
- Villaño, D., Fernández-Pachón, M.S., Troncoso, A.M., García-Parrilla, M.C., 2006. Influence of enological practices on the antioxidant activity of wines. *Food Chem.* 95, 394–404. <https://doi.org/10.1016/j.foodchem.2005.01.005>.
- Walker, E.B., 2007. HPLC analysis of selected xanthenes in mangosteen fruit. *J. Sep. Sci.* 30, 1229–1234. <https://doi.org/10.1002/jssc.200700024>.

- Wang, M.-H., Zhang, K.-J., Gu, Q.-L., Bi, X.-L., Wang, J.-X., 2017. Pharmacology of mangostins and their derivatives: a comprehensive review. *Chin. J. Nat. Med.* 15, 81–93. [https://doi.org/10.1016/S1875-5364\(17\)30024-9](https://doi.org/10.1016/S1875-5364(17)30024-9).
- Wittenauer, J., Falk, S., Schweiggert-Weisz, U., Carle, R., 2012. Characterisation and quantification of xanthenes from the aril and pericarp of mangosteens (*Garcinia mangostana* L.) and a mangos-teen containing functional beverage by HPLC–DAD–MSn. *Food Chem.* 134, 445–452. <https://doi.org/10.1016/j.foodchem.2012.02.094>.
- Xu, X.-H., Liu, Q.-Y., Li, T., Liu, J.-L., Chen, Xin, Huang, L., Qiang, W.-A., Chen, Xiuping, Wang, Y., Lin, L.-G., Lu, J.-J., 2017. Garcinone E induces apoptosis and inhibits migration and invasion in ovarian cancer cells. *Sci. Rep.* 7, 10718. <https://doi.org/10.1038/s41598-017-11417-4>.
- Yang, R., Li, P., Li, N., Zhang, Q., Bai, X., Wang, L., Xiao, Y., Sun, L., Yang, Q., Yan, J., 2017. Xanthenes from the Pericarp of *Garcinia mangostana*. *Mol. Basel Switz.* 22. <https://doi.org/10.3390/molecules22050683>.
- Yusuf, M., 2017. Agro-industrial waste materials and their recycled value-added applications: review. In: Martínez, L.M.T., Kharissova, O.V., Kharisov, B.I. (Eds.), *Handbook of Ecomaterials*. Springer International Publishing, Cham, pp. 1–11. [https://doi.org/10.1007/978-3-319-48281-1\\_48-1](https://doi.org/10.1007/978-3-319-48281-1_48-1).
- Zhou, S., Yotsumoto, H., Tian, Y., Sakamoto, K., 2021.  $\alpha$ -Mangostin suppressed melanogenesis in B16F10 murine melanoma cells through GSK3 $\beta$  and ERK signaling pathway. *Biochem. Biophys. Rep.* 26, <https://doi.org/10.1016/j.bbrep.2021.100949> 100949.